ELSEVIER

Biochimica et Biophysica Acta 1564 (2002) 333–342

BIOCHIMICA ET BIOPHYSICA ACTA
BBA

www.bba-direct.com

Analysis of membrane topology of the human reduced folate carrier protein by hemagglutinin epitope insertion and scanning glycosylation insertion mutagenesis

Xiang Y. Liu [a], Larry H. Matherly [a,b,c,*]

[a] *Cancer Biology Graduate Program, Barbara Ann Karmanos Cancer Institute, Wayne State University School of Medicine, Detroit, MI, USA*
[b] *Department of Pharmacology, Barbara Ann Karmanos Cancer Institute, Wayne State University School of Medicine, Detroit, MI, USA*
[c] *Experimental and Clinical Therapeutics Program, Barbara Ann Karmanos Cancer Institute, Wayne State University School of Medicine, 110 E. Warren Ave., Detroit, MI, USA*

Received 11 March 2002; received in revised form 14 May 2002; accepted 24 May 2002

Abstract

The human reduced folate carrier (RFC) is the major membrane transport system for both reduced folates and chemotherapeutic antifolate drugs, such as methotrexate (MTX). Although the RFC protein has been subjected to intensive study in order to identify critical structural and functional determinants of transport, it is impossible to assess the significance of these studies without characterizing the essential domain structure and membrane topology. The primary amino acid sequence from the cloned cDNAs predicts that the human RFC protein has 12 transmembrane domains (TMDs) with a large cytosolic loop between TMDs 6 and 7, and cytosolic-facing N- and C-termini. To establish the RFC membrane topology, a hemagglutinin (HA) epitope was inserted into the individual predicted intracellular and extracellular loops. HA insertions into putative TMD interconnecting loops 3/4, 6/7, 7/8, and 8/9, and the N- and C-termini all preserved MTX transport activity upon expression in transport-impaired K562 cells. Immunofluorescence detection with HA-specific antibody under both permeabilized and non-permeabilized conditions confirmed extracellular orientations for loops 3/4 and 7/8, and cytosolic orientations for loops 6/7 and 8/9, and the N- and C-termini. Insertion of a consensus *N*-glycosylation site [NX(S/T)] into putative loops 5/6, 8/9, and 9/10 of deglycosylated RFC-Gln^{58} had minimal effects on MTX transport. Analysis of glycosylation status on Western blots suggested an extracellular orientation for loop 5/6, and intracellular orientations for loops 8/9 and 9/10. Our findings strongly support the predicted topology model for TMDs 1–8 and the C-terminus of human RFC. However, our results raise the possibility of an alternative membrane topology for TMDs 9–12.

Keywords: Reduced folate carrier; Methotrexate; Topology; Epitope insertion; Site-directed mutagenesis

1. Introduction

The reduced folate carrier (RFC) is the transport system for reduced folates, including 5-methyl and 5-formyl tetrahydrofolate (H_4PteGlu), and antifolate drugs such as methotrexate (MTX) used for cancer chemotherapy [1,2]. The carrier is considered to be ubiquitously expressed in tissues and tumors and, by all indications, is the major folate transport mechanism in mammals [1,2].

Since the RFC was originally cloned from mouse and hamster cells in 1994 [3,4], and in human cells in 1995 [5–8], there has been an intensive effort to identify the critical structural and functional determinants of transport, using random chemical [9] and site-directed mutagenesis [10–12], or in vitro selection of drug-resistant cells with impaired RFC activity [13]. An impressive number of amino acids have been implicated as critical to RFC transport (numbers refer to the human RFC or hRFC), including glycine-44 [14], glutamate-45 [13,15], serine-46 [16], isoleucine-48 [17], aspartate-88 [12], serine-127 [14], alanine-132 [18], and arginines-133 [11,12] and -373 [11]. However, it is nearly impossible to assess the functional significance of these amino acids without a comprehensive model of RFC membrane topology that depicts key structural and functional domains including those comprising the putative

* Corresponding author. Experimental and Clinical Therapeutics Program, Barbara Ann Karmanos Cancer Institute, Wayne State University School of Medicine, 110 E. Warren Ave., Detroit, MI, USA. Tel.: +1-313-833-0715x2407; fax: +1-313-832-7294.
E-mail address: matherly@kci.wayne.edu (L.H. Matherly).

0005-2736/02/$ - see front matter © 2002 Elsevier Science B.V. All rights reserved.
PII: S0005-2736(02)00467-4

transmembrane "channel" for membrane traverse of hydrophilic folate and antifolate substrates.

In the original report of Dixon et al. [3], it was noted that RFC conformed to a topology computer model similar that for the glucose carrier (GLUT1), with up to 12 transmembrane domains (TMDs), a large cytosolic loop between TMDs 6 and 7, and cytosolic-facing N- and C-termini (Fig. 1 depicts this topology model for hRFC). For hRFC, glycosylation of asparagine-58 established this region as extracellular [19]. Moreover, a hemagglutinin (HA) peptide epitope (YPYDVPDYA) at the carboxyl terminus of hRFC expressed in transport-impaired K562 cells was inaccessible to HA-specific antibody without membrane permeabilization, thus establishing this region as intracellular [19]. More recently, Ferguson and Flintoff [20] used HA insertional mutagenesis and fluorescence staining to confirm other critical features of this model, including the cytosolic orientations of the amino terminus (proline-20) and the large connecting loop between TMDs 6 and 7 (serine-225), and an extracellular orientation for proline-297 in the connecting loop between TMDs 7 and 8. However, many other key features of the 12 TMD topology model have not been directly assessed or could not be confirmed due to a loss of hRFC expression and/or transport activity accompanying insertion of the HA peptide epitope [20].

In this report, we expand upon our previous studies [19] and those of Ferguson and Flintoff [20] in experimentally confirming the membrane topology of hRFC. We use two highly complementary experimental strategies including (i) HA insertion mutagenesis and immunofluorescence staining with HA-specific antibody in permeabilized and non-permeabilized cells, essentially as in these earlier studies [19,20], and (ii) scanning glycosylation insertion mutagenesis of the non-glycosylated hRFC-Gln^{58} [19], followed by Western blotting to confirm glycosylation status. Although our results strongly support the predicted topology for TMDs 1–8 in hRFC (Fig. 1), our results raise the possibility of an alternative membrane topology for TMDs 9–12.

2. Materials and methods

2.1. Reagents

[3′,5′,7-^{3}H] MTX (20 Ci/mmol) was purchased from Moravek Biochemicals (Brea, CA). Unlabeled MTX was provided by the Drug Development Branch, National Cancer Institute, Bethesda, MD. Both labeled and unlabeled MTX were purified by HPLC prior to use [21]. Restriction and modifying enzymes were obtained from Promega (Madison, WI) or Roche (Indianapolis, IN). Synthetic oligonucleotides were obtained from Invitrogen (Carlsbad, CA). Tissue culture reagents and supplies were purchased from assorted vendors with the exception of iron-supplemented calf serum, which was from Hyclone Laboratories, Inc. (Logan, UT).

2.2. Cell culture

The MTX transport-deficient K500E subline was selected from wild-type K562 (American Type Culture Collection) and maintained in RPMI 1640 medium (Life Technologies, Inc.) containing 10% calf serum, 2 mM L-glutamine, 100 U/ml penicillin, and 100 μg/ml streptomycin, with 0.5 μM of MTX [19]. K500E cells were transfected with the wild-type (KS43) hRFC cDNA in pCDNA3 (designated pC43) to generate the K43-6 subline [22], with the hRFC-Gln^{58} in pCDNA3 (designated DG9) to generate KEDG9 cells [19], or with an hRFC construct including a carboxyl-terminal HA insertion in pCDNA3 (designated hRFC-HA12 in the present study) to generate K43^{HA12} cells (previously called HA8) [19]. All hRFC transfectants were

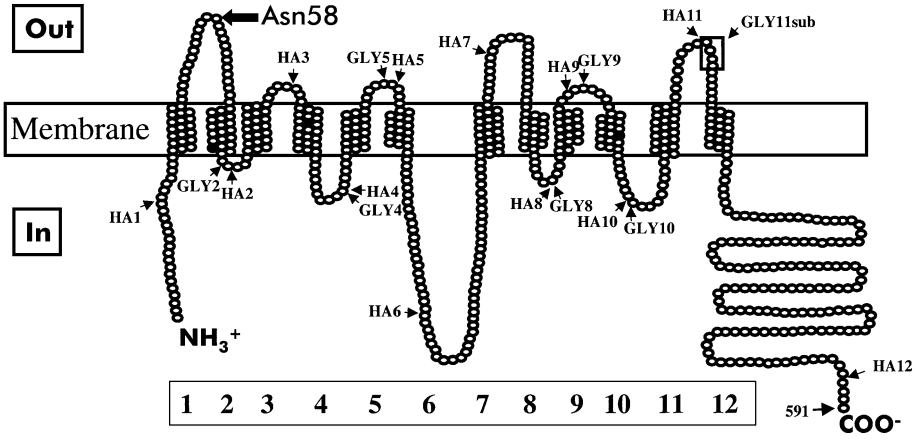

Fig. 1. Computer-predicted topology structure of the hRFC protein. A topology model for hRFC is shown depicting 12 TMDs (numbered 1–12), internally oriented amino and carboxyl termini, and an externally oriented *N*-glycosylation site at asparagine-58. The location of the HA- and *N*-glycosylation (GLY*n*) consensus insertions are indicated. The positions of these modifications are summarized in Tables 1–3. The solid circles designate conserved charged residues located in predicted TMD regions of hRFC and include asparate-88 (TMD2), arginine-133 (TMD4), and arginine-373 (TMD10).

cultured in complete RPMI 1640 medium plus 1 mg/ml G418 in a humidified atmosphere at 37 °C in the presence of 5% CO_2.

2.3. Site-directed mutagenesis

Two methods were used for site-directed mutagenesis.

(i) For the hRFC-HA3-11 constructs, a PCR-based mutagenesis kit (ExSite™, Stratagene) was used to insert a peptide including the HA epitope (YPYDVPDYAVN) into designated sites of hRFC (these are noted in Fig. 1 and summarized in Table 1). The VN residues were added to generate a unique *Hpa*I site (GTTAAC) in this series of constructs in order to confirm the presence of the HA peptide insertion. A highly processive polymerase, ExSite™ DNA polymerase (Stratagene), was used to eliminate possible random mutations induced by PCR. The full-length KS43 hRFC cDNA in pBluescript SK(−) (pKB43) [6] was amplified using the primers summarized in Table 1, following the procedure provided by the manufacturer. Insertion of the HA epitope was screened by either PCR, with primers specific for HA (HAtag, 5′ tacccatacgatgttccggattacgct3′ or rHAtag, 5′agcgtaatccggaacatcgtatgggta3′), or by *Hpa*I digestion (see above). The hRFC-HA3-11 inserts were cloned into pCDNA3 at the *Kpn*I and *Xba*I sites.

(ii) "Splicing by Overlap Extension" (SOE) PCR [23] was used to prepare hRFC-HA1 and -HA2 constructs and the *N*-glycosylation mutants (hRFC-GLY5, -GLY8, -GLY9, -GLY10, -GLY11), using the complementary PCR primers shown in Tables 1 and 2. For the HA insertion mutants, wild-type pC43 was used as template; for the glycosylation insertion mutants, the deglycosylated DG9 form of hRFC, with glutamine-58 replacing asparagine-58, in pCDNA3 [19] was used as template. For the hRFC-HA1, -HA2, and -GLY5, two PCR steps were initially performed to amplify two separate products, using the forward mutation primer (Primer 2) and the rHA-7 reverse primer (5′ctcgttccacaggatgtgcac3′; positions 882 to 862 relative to start codon ATG where A is number 1), and the reverse mutation primer (Primer 1) and p8 forward primer (5′cagtgtcaccttcgtcccctccg3′; positions −46 to −24). PCR conditions for the primary PCR reactions were 94 °C for 30 s, 56 °C for 30 s, and 72 °C for 60 s for 35 cycles. Secondary PCR was performed with the p8/rHA-7 primers and mixed primary PCR products as templates, using the same conditions as for the primary PCRs. The same strategy and PCR conditions were used to generate hRFC-GLY8, -GLY9, -GLY10, and -GLY11 mutations, however, KS2 (5′cgcagcctcttcttcaaccgc3′; positions 622 to 642) and RFCout12 (5′gacaaccccttcccccctgcactctgt3′; positions 1647 to 1619) primers were used with mutation primers 1 and 2, respectively (Table 2), for the primary PCR reactions. Secondary PCRs were performed with the KS2/RFCout12 primers. For subcloning the hRFC-HA1, -HA2, and hRFC-GLY5 mutant constructs, the secondary PCR products were digested with *Bbr*PI/*Not*I, purified, and ligated into the *Bbr*PI/*Not*I-digested pC43 or DG9 vectors, as appropriate, for transformation. *Not*I/*Sfi*I restriction sites were used to subclone the hRFC-GLY8, -GLY9, -GLY10, and -GLY11 (both *-ins* and *-sub* constructs) PCR products into digested DG-9 vector. All mutant hRFC constructs were confirmed by automated sequencing at the Center of Molecular Genetics sequencing facility (Wayne State University).

Mutant constructs (5 μg) were stably transfected into K500E cells with Lipofectin (Life Technologies). Mutant clones were selected for growth in 1 mg/ml G418 and isolated from 0.35% soft agar for expansion and screening. These methods are identical to those described in our previous report [19].

2.4. Western analysis of hRFC

Plasma membranes were prepared and membrane proteins were solubilized in 10 mM Tris–HCl, pH 7.0, with proteolytic inhibitors [24]. Aliquots were electrophoresed on 7.5% polyacrylamide gels in the presence of SDS [25]

Table 1
PCR primers for hRFC mutant constructs with HA insertions

hRFC-HA[a]	Insertion sites[b]	Primer 1[c]	Primer 2[d]
1	G17–P18	5′Zcccaggttccacgggcacctgctt3′	5′Xcctgaccccgagctccggtcctgg3′
2	Y92–T93	5′Zgtagcgcaggtagtcggtgag3′	5′Xacgccggtgctgctgctgcag3′
3	Q120–L121	5′ctgcatgtgcgccaccgagtg3′	5′Xctcatggagctcttctacagc3′
4	G154–Y155	5′gccggccacacgctggtagcgcgcgg3′	5′Xtactcgcgcgctgcggtgctgctgggcgtg3′
5	S183–T184	5′ggagaaggagactcggcccac3′	5′Xacgctcaactacatctcgctg3′
6	E226–L227	5′ctccgaagccgaggtttcgca3′	5′Xctggagcgcatgaatcccggc3′
7	E294–V295	5′ctcgttccacaggatgtgcac3′	5′Xgtggaccccaccaccaacagtg3′
8	A332–R333	5′cgcccagcggatcttcacgaa3′	5′Xcgctggtccaagctgctcatc3′
9	T356–R357	5′cgtgtgcgccagaaggaagaccagccccg3′	5′Xcgccacccgagcagcatctggctgtgcta3′
10	Q386–I387	5′ctgaaaggtggcgatgggcac3′	5′Xattgcatcttctctgtctaaa3′
11	L426–P427	5′gaggcccaggccccgcacgtc3′	5′Xccggtccgcaagcagttccag3′

[a] hRFC-HA constructs 1–11, as described in the text.
[b] Location of HA-VN (YPYDVPDYAVN) epitope insertion in hRFC primary sequence.
[c] Antisense primer where "Z" corresponds to gtt aac agc gta atc cgg aac atc gat.
[d] Sense primer where "X" corresponds to atc gat gtt ccg gat tac gct gtt aac.

Table 2
N-Glycosylation mutation primers

hRFC-GLY[a]	Insertion site[b]	Primer 1[c]	Primer 2[d]
2	R91–N–Y92	5′cagcaccggcgtgtag**gtt**gcgcaggtagtc3′	5′accgactacctgcgc**aac**tacacgccggtgctg3′
4	G154N	5′cgcagcgcgcgagtc**gtt**ggccacacgatggta3′	5′taccaacgtgtggcc**aac**tactcgcgcgctgcg3′
5	F182N	5′gtagttgagcgtggag**gtt**ggagactcggcccac3′	5′gtgggccgagtctcc**aac**tccacgctcaactac3′
8	R333N	5′gagcagcttggaccag**gtt**cgcccagcggatctt3′	5′aagatccgctgggcg**aac**tggtccaagctgctc3′
9	H358N	5′ccagatgctgctcgg**gtt**gcgcgtgtgggccag3′	5′ctggcccacacgcgc**aac**ccgagcagcatctgg3′
10	I387N	5′agacagagaagatgc**att**ctgaaaggtggcgat3′	5′atcgccacctttcag**aat**gcatcttctctgtct3′
11*sub*[e]	PVRK430*NNST*	5′gaactg**actagtgttgtt**gaggcccaggccccgcacgtc3′	5′ggcctc**aacaacactagt**cagttccagttatactccgtg3′
11*ins*[e]	V428–*NNST*–R429	5′cttgcg**actagtgttatt**gaccgggaggcccaggcccc3′	5′ccggtc**aataacactagt**cgcaagcagttccagttatac3′

[a] hRFC-GLY constructs, as described in the text.
[b] Location of *N*-glycosylation [NX(S/T)] concensus sequence in the hRFC primary sequence.
[c] Antisense primer.
[d] Sense primer.
[e] In GLY11*sub*, residues PVRK (positions 427–430) were substituted by NNST, whereas in GLY*ins*, NNST was inserted after position 428.

and electroblotted onto PVDF membranes (Pierce) [26]. hRFC proteins were detected by enhanced chemiluminescence (Roche) with protein A-purified hRFC-specific antibody generated in rabbits with a glutathione S-transferase (GST)-hRFC fusion protein [14].

2.5. Immunofluorescence microscopy

The orientations of HA epitope in assorted hRFC-HA proteins in transfected cells were determined by immunofluorescence using the HA-specific rhodamine-conjugated 12CA5 antibody (Roche). Non-permeabilized cells were first incubated with rhodamine-conjugated 12CA5 in RPMI 1640 medium, containing 10% calf serum, 2 mM L-glutamine, 100 U/ml penicillin, and 100 μg/ml streptomycin for 1 h at 4 °C. The cells were fixed in 3.3% paraformaldehyde in PBS for 30 min on ice. For permeabilization, cells were washed with ice-cold PBS twice and resuspended in 1 ml of 3.3% paraformaldehyde and fixed for at least 30 min on ice. Cells were then treated with 0.1% Triton X-100 in PBS for 5 min on ice, washed twice with large volumes (~15 ml) of PBS, and then blocked with 1% BSA in PBS for 1.5 h at 4 °C. Cells were incubated in 200 μl PBS containing 5 μg/ml of rhodamine-conjugated 12CA5 antibody and 1% BSA for 1 h at 4 °C. Both permeabilized and non-permeabilized cells were washed three times with PBS. Cells were cytocentrifuged onto microscope slides, mounted with "SlowFade" antifade reagent (Molecular Probes) and sealed with cover slips. Immunofluorescence microscopy was performed with an Olympus BX40 fluorescence microscope using an Uplan F1 40×/0.75 object lens. Pictures were taken by a Sony DXC-970MD 3CCD color video camera connected to an NEC Express 5800 computer for image visualizing.

2.6. Membrane transport measurements

Initial rates of [^{3}H]-MTX (0.5 μM) uptake were measured over 180 s, as previously described [6,12,22]. Levels of intracellular radioactivity were expressed as picomoles per milligram of protein, calculated from direct measurements of radioactivity and protein contents of the cell homogenates. Protein assays were performed with the method of Lowry et al. [27].

3. Results

3.1. Expression of hRFC-HA and hRFC-GLY constructs in transport-impaired K562 cells

A computer-generated topology model based on the predicted hRFC amino acid sequence is shown in Fig. 1. The hydropathy analysis ("TMPRED"; [28]) for hRFC predicts a model expected for an integral membrane protein with up to 12 stretches of 17–25 mostly hydrophobic, alpha helix-promoting amino acids (Fig. 1). In support of this model are the findings that asparagine-58 was glycosylated [22], and that a carboxyl terminal HA-tag (i.e., hRFC-HA12) was not accessible to 12CA5 antibody labeling without membrane permeabilization [19,20]. Other features of this model have been confirmed by HA insertion mutagenesis and immunofluorescence staining [20], and include cytosolic orientations of the amino terminus (proline-20) and the large connecting loop between TMDs 6 and 7 (serine-225), and an extracellular orientation for proline-297 in the connecting loop between TMDs 7 and 8.

To verify features of this model that were not previously assessed or could not be confirmed, two complementary approaches were used. (i) HA epitopes were inserted into the predicted loops connecting TMDs in hRFC to generate the hRFC-HA2, hRFC-HA3, hRFC-HA4, hRFC-HA5, hRFC-HA8, hRFC-HA9, hRFC-HA10, and hRFC-HA11 constructs (Fig. 1 and Table 1). Constructs hRFC-HA1, hRFC-HA6, hRFC-HA7, and hRFC-HA12 (Fig. 1) were also prepared, essentially corresponding to those reported by Ferguson and Flintoff [20] to restore hRFC transport activity in transfected Chinese hamster ovary cells. (ii) Scanning *N*-glycosylation insertion mutagenesis (Table 2) was used with the hRFC DG-9 construct encoding hRFC-Gln^{58} [19] to generate hRFC-GLY2, hRFC-GLY4, hRFC-GLY5, hRFC-

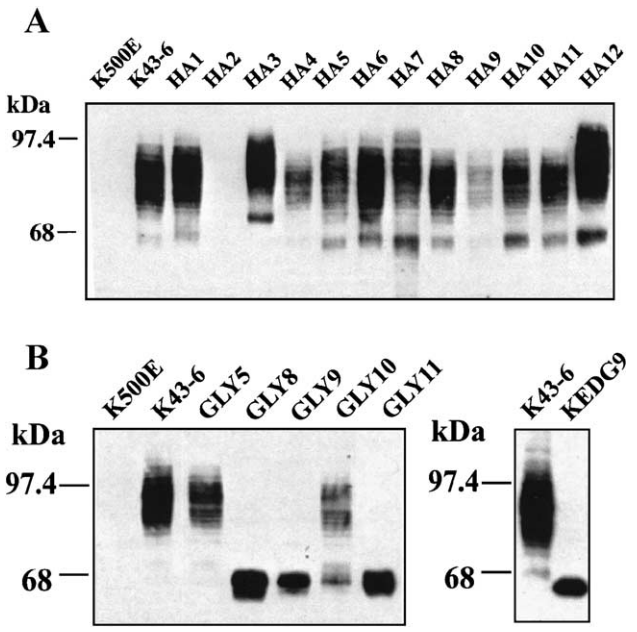

Fig. 2. Expression of hRFC-HA and -GLY mutant constructs in transport-impaired K562 cells. Data are shown for a Western blot of plasma membrane proteins from hRFC-deficient K500E cells and K500E transfectants expressing wild-type hRFC (K43-6) and mutant hRFCs including hRFC-HA1 through -HA12 (panel A), and hRFC-GLY5 through -GLY11 (panel B). In the right portion of panel B are shown results for the migration of the deglycosylated hRFC-Gln^{58} construct (KEDG9 cells) for comparison with the wild-type hRFC construct in K43-6 cells. hRFC-GLY11 refers to the GLY11*sub* mutation, as described in Table 2. Twenty micrograms of protein from each sample were separated on a 7.5% gel in the presence of SDS and electroblotted onto a PVDF membrane. Detection was with anti-hRFC antibody and enhanced chemiluminescence. Molecular weight standards (in kDa) are shown.

GLY8, hRFC-GLY9, hRFC-GLY10, and hRFC-GLY11*sub* [19]. As previously reported, replacement of the consensus *N*-glycosylation site at asparagine-58 with glutamine had no adverse effect on plasma membrane targeting or transport function of hRFC [19].

The mutant constructs were all transfected into transport-impaired K562 human cells (K500E), characterized by a nearly complete loss of hRFC protein and MTX transport [29]. Stable transfectants (designated K43^{HAn} and K43^{GLYn}, for the series of HA-tagged and GLY-insertion constructs, respectively) were selected in G418 selection medium, and clonal populations expanded and screened on Western blots with hRFC-specific antiserum.

Fig. 2A and B show that all mutants, with the exception of K43^{HA2}, expressed high levels of hRFC protein. For all of the HA-tagged constructs, hRFC migrated as a broadly banding species centered at ~85 kDa (Fig. 2A). However, among the expressed hRFC-GLY constructs, the pattern of protein banding differed and either resembled that for the glycosylated wild-type protein in K43-6 cells (for hRFC-GLY5 and -GLY10) or the deglycosylated carrier in KEDG9 cells (for hRFC-GLY8, 9, and 11*sub*) [19] (Fig. 2B). Mutants hRFC-GLY2 (R91–N–Y92) and hRFC-GLY4 (G154N) failed to produce detectable hRFC protein on western blots (data not shown). Thus, the vast majority of HA- and *N*-glycosylation insertions did not significantly interfere with hRFC expression or plasma membrane targeting. The lack of expression with hRFC-HA2, hRFC-GLY2, and hRFC-GLY4 proteins likely reflects misfolding of the mutant proteins resulting in increased rates of degradation [14,30].

All of the expressed hRFC forms were tested for transport activity using ^{3}H-MTX as substrate for comparison with non-transfected K500E cells, and K43^{HA12} (expresses carboxyl HA-tagged hRFC) and K43-6 (expresses wild-type hRFC) cells, both of which exhibit high levels of ^{3}H-MTX transport [19,22]. For the series of hRFC-HA constructs, including hRFC-HA1, -HA3, -HA6, -HA7, and -HA8, MTX transport was increased over that in hRFC-null K500E cells and was 20–60% of that in K43^{HA12} cells (Fig. 3A). However, for hRFC-HA4, -HA5, -HA9, -HA10,

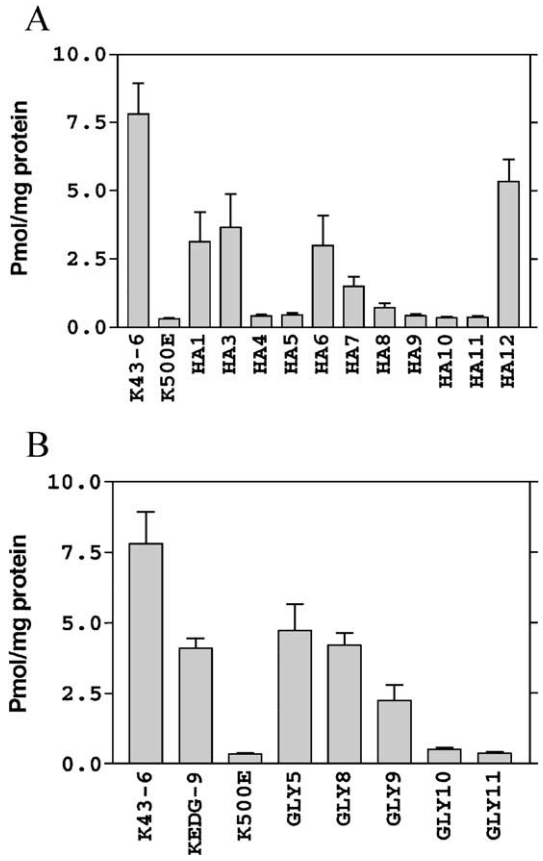

Fig. 3. Rates of ^{3}H-MTX transport in K562 transfectants expressing wild-type and mutant hRFC-HA and hRFC-GLY proteins. ^{3}H-MTX (0.5 μM) uptakes were measured for 180 s at 37 °C. Panel A shows data for hRFC-HA transfectants and panel B shows uptake rates for the hRFC-GLY transfectants. For comparison, transport data are shown for wild-type hRFC transfectants (i.e., K43-6) and hRFC-Gln^{58} transfected cells (KEDG9). For this series of experiments, hRFC-GLY11 refers to the GLY11*sub* mutation, as described in Table 2. All transport results are the mean values of three to four separate experiments (±S.E.).

and -HA11, levels of ^{3}H-MTX uptake were not significantly different from that in K500E cells.

For the hRFC-GLY series of transfectants, high levels of MTX transport were, likewise, detected for K43^{GLY5} (hRFC-GLY5), K43^{GLY8} (hRFC-GLY8), and K43^{GLY9} (hRFC-GLY9) cells (Fig. 3B). Transport in K43^{GLY10} cells (hRFC-GLY10) was indistinguishable from that in K500E cells. Two hRFC-GLY11 mutant constructs were generated, one (hRFC-GLY11*sub*) in which the *N*-glycosylation consensus sequence NNST replaced four non-conserved amino acids (P^{427}VRK) in the middle part of the TMD 11/12 connecting loop and another (hRFC-GLY11*ins*) in which NNST was inserted into the middle part of loop 11 between positions V^{428} and P^{429}. Both constructs were expressed, yet neither was functional for MTX transport (the data in Figs. 2 and 3 are for the hRFC-GLY11*sub*).

3.2. Analysis of HA epitope membrane orientation in hRFC-HA mutant proteins by immunofluorescence microscopy

Stable transfectants with high level expression of functional HA epitope-tagged hRFCs were assayed by immunofluorescence staining with rhodamine-conjugated 12CA5 antibody with and without membrane permeabilization, essentially as described by Ferguson and Flintoff [20]. Without permeabilization, fluorescence should be detectable in transfectants expressing hRFC-HA constructs for which the HA tag was localized on the outside (extracellular) surface of cells. However, when the HA tag was localized to the inside (cytosolic) face, permeabilization would be necessary to detect the fluorescent antibody complex.

Data are shown in Fig. 4 for transfected cells expressing the functional hRFC-HA1, -HA3, -HA6, -HA7, -HA8, and -HA12 constructs, along with that for mock-transfected K500E cells as a negative control. Fluorescence was detected in all permeabilized cells (denoted with "*p*" as in "HA1*p*"), with the exception of K500E cells, thus demonstrating good accessibility and reactivity of 12CA5 antibody to the membrane-localized HA-tagged hRFC proteins.

For hRFC-HA3 and -HA7, the HA epitopes were clearly extracellular since fluorescence was detectable *without* permeabilization. However, for hRFC-HA1, -HA6, -HA8, and -HA12, permeabilization was essential to detect the HA epitope (Fig. 4), demonstrating a lack of accessibility to antibody and a probable cytosolic orientation for the HA epitope.

3.3. Topology mapping by analysis of glycosylation patterns in hRFC glycosylation insertion mutants

Scanning glycosylation mutagenesis, in which an *N*-glycosylation [NX(S/T)] consensus sequence is inserted at different sites along a primary sequence, has been successfully used for epitope mapping of integral membrane proteins [31]. The underlying premise behind this approach involves the notion that glycosylation occurs exclusively on the luminal side of endoplasmic reticulum (ER) membranes [32]. Once the protein is transported to the plasma membrane, the luminal side of the ER corresponds to the extracellular face of the protein so that the presence of an *N*-linked oligosaccharide at a particular NX(S/T) consensus sequence establishes its extracellular orientation.

For hRFC, glycosylation resulted in a marked shift in banding on Western blots from the ~65 kDa for the hRFC-Gln^{58} construct expressed in KEDG9 cells [19] to a broadly migrating band centered at ~85 kDa for wild-type hRFC

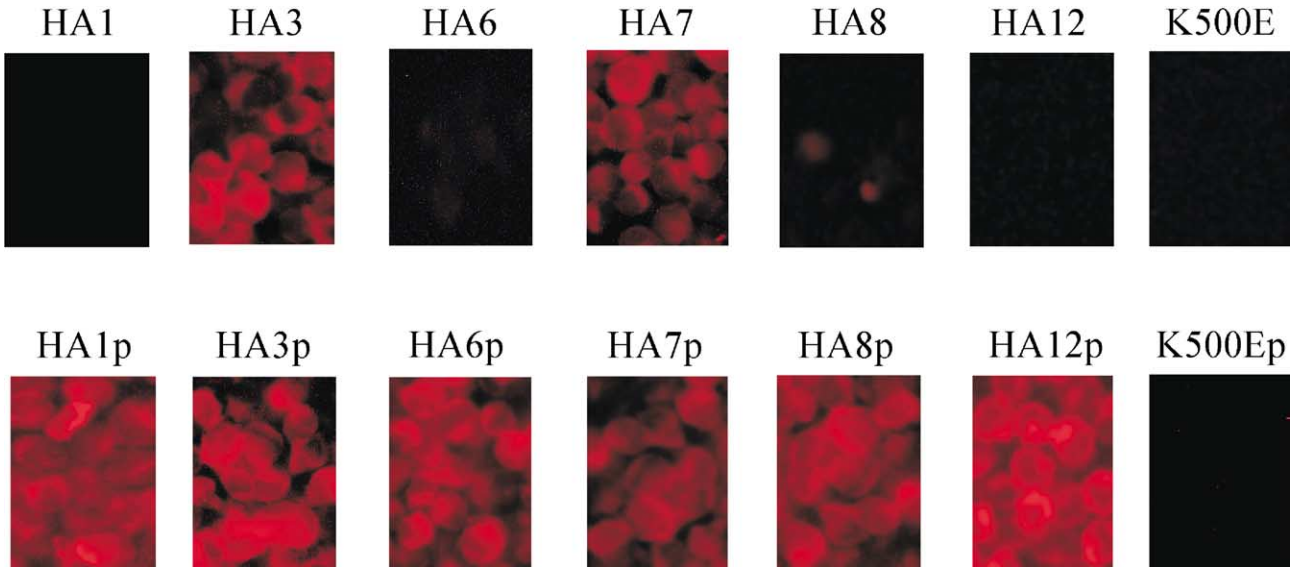

Fig. 4. Detection of HA epitope-tagged hRFC proteins by immunofluorescence staining. Mock- and transport-competent hRFC-HA-transfected K500E cells were incubated with rhodamine-conjugated anti-HA antibody (12CA5) with ("*p*" as in HA*np*) or without pretreatment with Triton X-100, as described in the text.

in K43-6 cells (Fig. 2B). Both hRFC-GLY5 and -GLY10 were glycosylated on Western blots, establishing extracellular orientations for the glycosylation consensus sequences inserted at positions 182 and 387. However, only hRFC-GLY5 was functional (Fig. 3). hRFC-GLY5 and hRFC-GLY10 could be enzymically deglycosylated to their 65 kDa forms by *N*-glycosidase F (data not shown). The lack of glycosylation for hRFC-GLY8 and hRFC-GLY9 (Fig. 2B) is consistent with an intracellular orientation for positions 333 and 358.

4. Discussion

Hydropathy analysis of RFC from both humans and rodents has resulted in a topology model involving up to 12 TMDs, symmetrically grouped around a large central loop with internally oriented amino- and carboxyl termini [1,3,20]. In this study, we performed a systematic investigation of hRFC membrane topology in an attempt to verify this model. We employed two highly complementary approaches, HA insertion mutagenesis and immunofluorescence staining with HA-specific antibody in permeabilized and non-permeabilized human transfectants, and scanning glycosylation insertion mutagenesis of the non-glycosylated hRFC-Gln^{58} construct, followed by Western blotting to confirm glycosylation status and probable membrane orientation. We focused primarily on *functional* hRFC constructs in our analysis to exclude any significant bias that may result from misfolded non-functional proteins.

Both HA-epitope insertion and scanning glycosylation mutagenesis have been used to characterize the membrane topologies for a number of integral membrane proteins including the glycine transporter [33], human glucose 6-phosphate transporter [34], Band 3 anion exchanger [31], mouse P-glycoprotein [35], and Na^+K^+ ATPase [36]. Moreover, for hRFC, HA insertion mutagenesis was used to establish the topologies for the N- and C-termini, and the connecting loops between TMDs 6 and 7, and between TMDs 7 and 8 [19,20]. The present results strongly support the computer-predicted topology model for TMDs 1–8 (Fig. 1). However, the topology for TMDs 9–12 remains unsettled. Our findings are summarized in Table 3, and are interpreted as follows.

4.1. TMDs 1–8 and central connecting loop

Insertion of the HA epitope at glycine-17 caused no adverse effects on hRFC expression and function. The resulting hRFC-HA1 protein was inaccessible to 12CA5 antibody without permeabilization, confirming the cytosolic orientation of the N-terminal HA epitope, as previously reported [20]. Our earlier finding that hRFC is glycosylated at asparagine-58 [19] established an extracellular orientation for the connecting loop between putative TMDs 1 and 2. While hRFC-HA2 (HA insertion at tyrosine-92) could not be stably expressed in K500E cells, hRFC-HA3 (insertion at glutamine-120) was highly expressed and was competent for MTX uptake. By immunofluorescence staining, the HA orientation in hRFC-HA3 was unambiguously extracellular. The insertion of the HA epitope at serine-183 in hRFC-HA5 abolished carrier activity, however, replacement of phenylalanine-182 by asparagine in hRFC-GLY5 generated a new *N*-glycosylation consensus site and resulted in the synthesis

Table 3
Summary of HA-epitope insertion and scanning *N*-glycosylation data

Number[a]	HA Insertion between	GLY Insertion	Location	Transport[b]		Prediction[c]	Experimental[d]	
				HA	GLY		HA	GLY
1	G17–P18		N-terminus	Y	ND	C	C	
2	Y92–T93	R91–N–Y92	TMD2/3	NE	NE	C	–	–
3	Q120–L121		TMD3/4	Y	ND	E	E	
4	G154–Y155	G154N	TMD4/5	N	NE	C	–	–
5	S183–T184	F182N	TMD5/6	N	Y	E	–	E
6	E226–L227		TMD6/7	Y	ND	C	C	
7	E294–V295		TMD7/8	Y	ND	E	E	
8	A332–R333	R333N	TMD8/9	Y	Y	C	C	C
9	T356–R357	H358N	TMD9/10	N	Y	E	–	C
10	Q386–I387	I387N	TMD10/11	N	N	C	–	–
11*sub*[e]	L426–P427	PVRK430*NNST*	TMD11/12	N	N	E	–	–
11*ins*[e]		V428–*NNST*–R429						
12	Q587–N588		C-terminus	Y	ND	C	C	–

Abbreviations: TMD, transmembrane domain; Y, yes; N, no; NE, not expressed; C, cytosolic; E, extracellular; NE, not expressed; ND, not determined.

[a] Numbers refer to HA or GLY constructs, as shown in Fig. 1.

[b] Transport activity was measured over 180 s with 0.5 μM MTX, as described in Materials and methods.

[c] Based on the 12-TMD model for hRFC topology depicted in Fig. 1.

[d] Experimentally determined topology by fluorescence staining (HA) or Western analysis (GLY) for the transport competent hRFC constructs, as described in the text.

[e] In GLY11*sub*, residues PVRK (positions 427–430) were substituted by NNST. In GLY*ins*, NNST was inserted after position 428.

of a functional glycosylated hRFC protein. Thus, the loop between TMDs 5 and 6 must be extracellular.

Similar to the results of Ferguson and Flintoff [20], neither insertion of the HA epitope at glutamate-226 in the loop connecting TMDs 6 and 7, nor at glutamate-294, between TMDs 7 and 8, significantly interfered with hRFC transport function. By immunofluorescence staining, these regions mapped to the cytosolic and extracellular faces, respectively. Finally, insertion of an HA epitope at alanine-332 (in hRFC-HA8), between TMDs 8 and 9, preserved low levels of transport activity and resulted in a pattern of antibody reactivity consistent with a cytosolic orientation. This interpretation was strengthened by the complete absence of glycosylation in the highly active hRFC-GLY8 protein (replacement of arginine-333 by asparagine). Collectively, these results support the predicted membrane topology for TMDs 1–8 depicted in Fig. 1.

Additional evidence for the predicted topology model involves loss of transport activity upon generation of energetically unfavored "uncompensated" charged residues in hydrophobic domains [37], by neutralizing one-half of a charge pair [38–42]. For instance, replacement of aspartate-88 and arginine-133 in hRFC by neutral amino acids, individually (valine and leucine, respectively), abolished transport [12]. However, their simultaneous replacement restored activity, establishing their charge-pair stabilization and probable localization in membrane-spanning domains (TMDs 2 and 4, respectively, in Fig. 1).

4.2. TMDs 9–12 and carboxyl terminus

Interpretation of the topology for TMDs 9–12 is confounded by the lack of functional hRFC-HA9, -HA10, -HA11, -GLY10, and -GLY11 proteins. hRFC-GLY9 and hRFC-HA12 were both functional. hRFC-GLY9 was unglycosylated, and hRFC-HA12 required permeabilization for 12CA5 antibody labeling, suggesting intracellular orientations for the connecting loop between TMD 9 and TMD 10, and the carboxyl terminus. However, the surprising lack of glycosylation of the TMD 9/10 loop in hRFC-GLY9 may also reflect *spacial* considerations for which the *N*-glycosylation consensus sequence may be simply too close to the end of a transmembrane segment for proper *N*-glycosylation by oligosaccharyl transferase [31]. By analogy with aspartate-88/arginine-133 [12] (see above), the loss of transport activity by neutralizing arginine-366 with leucine in murine RFC (arginine-373 in hRFC; located in putative TMD 10 in Fig. 1) [11] may involve the generation of an uncompensated anionic residue in a hydrophobic domain.

These results are not easily reconciled with the computer-predicted topology model (Model A, Fig. 5) for TMDs 7–12 and are best explained by alternative models (Models B1 and B2, Fig. 5). For the latter, TMD 8 spans the plasma membrane, as for Model A, yet both the original TMD 8/9 and TMD 9/10 connecting loops are intracellular. Although the dispositions of the original TMDs 9 through 12 are not completely certain, glutamate-373 in TMD 10 appears to be buried (see above), leading us to depict TMD 10 as spanning the plasma membrane. It is of interest that models B1 and B2 both predict that position 387 in the original TMD 10/11 connecting loop has an extracellular orientation, given the finding that asparagine-387 in hRFC-GLY10 was glycosylated. However, hRFC-GLY10 was non-functional. Since the carboxyl terminus of hRFC is intracellular, either the original TMD 12 (model B1) or TMD 11 (model B2) must also span the membrane.

Although both models B1 and B2 predict only 10 TMDs, from the marked hydrophobicities of the original TMDs 9–12, some degree of membrane association with all these domains, nonetheless, seems likely. A "membrane embedded" hydrophobic domain structure analogous to TMDs 9 and 11 in model B1, and TMDs 9 and 12 in model B2, was described for the topology of the Alzheimer's disease-related presenilin 1 protein [43]. Moreover, similar membrane localized "reentrant loop" structures were described for the glutamate transporter family [44,45].

Further clarification of the membrane topology of hRFC will undoubtedly require alternative experimental approaches

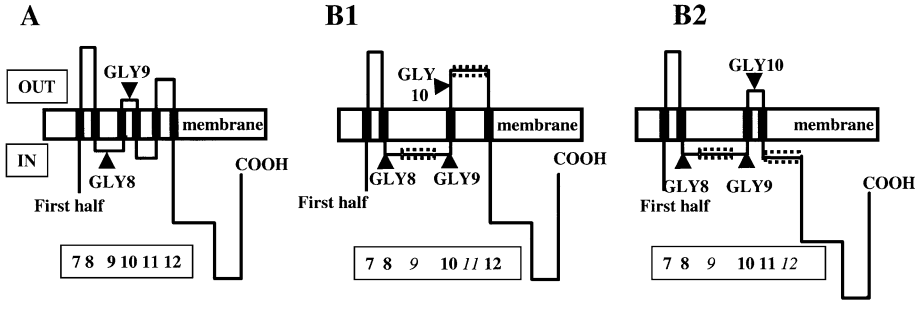

Fig. 5. Proposed models of hRFC topology for TMDs 7–12. Three topology schemes for hRFC are presented for TMDs 7–12. Model A is based on the 12 TMD model in Fig. 1. Alternative models B1 and B2 are based on the lack of glycosylation for asparagine-358 for hRFC-GLY9, suggesting that the original TMD 9/10 connecting loop has an intracellular orientation, and the presumption of a membrane-spanning TMD 10 including arginine-373. These models are further supported by the finding that asparagine-387 in hRFC-GLY10 is glycosylated, as described in the text. Models B1 and B2 differ by virtue of the presence of membrane-spanning TMD 12 and TMD 11, respectively. For model B1, TMDs 9 and 11 (depicted by broken lines) are viewed as membrane-embedded hydrophobic domains; for model B2, TMDs 9 and 12 (broken lines) are the membrane-embedded domains.

(e.g., cysteine-scanning mutagenesis and reactivity with *N*-biotinylaminoethyl methanethiosulfonate [46]). Clarification of the membrane topology and domain structure of hRFC is requisite to understanding the molecular mechanism of folate and antifolate membrane transport.

Acknowledgements

This study was supported by grant CA53535 from the National Cancer Institute, National Institutes of Health.

References

[1] F.M. Sirotnak, B. Tolner, Carrier-mediated membrane transport of folates in mammalian cells, Annu. Rev. Nutr. 19 (1999) 91–122.
[2] L.H. Matherly, Molecular and cellular biology of the human reduced folate carrier, Prog. Nucleic Acid Res. Mol. Biol. 67 (2001) 131–162.
[3] K.H. Dixon, B.C. Lanpher, J. Chiu, K. Kelley, K.H. Cowan, A novel cDNA restores reduced folate carrier activity and methotrexate sensitivity to transport deficient cells, J. Biol. Chem. 269 (1994) 17–20.
[4] F.M. Williams, R.C. Murray, T.M. Underhill, W.F. Flintoff, Isolation of a hamster cDNA clone coding for a function involved in methotrexate uptake, J. Biol. Chem. 269 (1994) 5810–5816.
[5] F.M. Williams, W.F. Flintoff, Isolation of a human cDNA that complements a mutant hamster cell defective in methotrexate uptake, J. Biol. Chem. 270 (1995) 2987–2992.
[6] S.C. Wong, S.A. Proefke, A. Bhushan, L.H. Matherly, Isolation of human cDNAs that restore methotrexate sensitivity and reduced folate carrier activity in methotrexate transport-defective Chinese hamster ovary cells, J. Biol. Chem. 270 (1995) 17468–17475.
[7] J.A. Moscow, M. Gong, R. He, M.K. Sgagias, K.H. Dixon, S.L. Meltzer, P.S. Meltzer, K.H. Cowan, Isolation of a gene encoding a human reduced folate carrier (RFC1) and analysis of its expression in transport-deficient, methotrexate-resistant human breast cancer cells, Cancer Res. 55 (1995) 3790–3794.
[8] P.D. Prasad, S. Ramamoorthy, F.H. Leibach, V. Ganapathy, Molecular cloning of the human placental folate transporter, Biochem. Biophys. Res. Commun. 206 (1995) 681–687.
[9] R. Zhao, I.G. Sharina, I.D. Goldman, Pattern of mutations that results in loss of reduced folate carrier function under antifolate selective pressure augmented by chemical mutagenesis, Mol. Pharmacol. 56 (1999) 68–76.
[10] R. Zhao, F. Gao, P.J. Wang, I.D. Goldman, Role of the amino acid 45 residue in reduced folate carrier function and ion-dependent transport as characterized by site-directed mutagenesis, Mol. Pharmacol. 57 (2000) 317–323.
[11] I.G. Sharina, R. Zhao, Y. Wang, S. Babani, I.D. Goldman, Mutational analysis of the functional role of conserved arginine and lysine residues in transmembrane domains of the murine reduced folate carrier, Mol. Pharmacol. 59 (2001) 1022–1028.
[12] X.Y. Liu, L.H. Matherly, Functional interactions between arginine-133 and aspartate-88 in the human reduced folate carrier: evidence for a charge-pair association, Biochem. J. 358 (2001) 511–516.
[13] R. Zhao, Y.G. Assaraf, I.D. Goldman, A mutated murine reduced folate carrier (RFC1) with increased affinity for folic acid, decreased affinity for methotrexate, and an obligatory anion requirement for transport function, J. Biol. Chem. 273 (1998) 19065–19071.
[14] S.C. Wong, L. Zhang, T.L. Witt, S.A. Proefke, A. Bhushan, L.H. Matherly, Impaired membrane transport in methotrexate-resistant CCRF-CEM cells involves early translation termination and increased turnover of a mutant reduced folate carrier, J. Biol. Chem. 274 (1999) 10388–10394.
[15] G. Jansen, R. Mauritz, S. Drori, H. Sprecher, I. Kathmann, M. Bunni, D.G. Priest, P. Noordhuis, J.H. Schornagel, H.M. Pinedo, G.J. Peters, Y.G. Assaraf, A structurally altered human reduced folate carrier with increased folic acid transport mediates a novel mechanism of antifolate resistance, J. Biol. Chem. 273 (1998) 30189–30198.
[16] R. Zhao, Y.G. Assaraf, I.D. Goldman, A reduced folate carrier mutation produces substrate-dependent alterations in carrier mobility in murine leukemia cells and methotrexate resistance with conservation of growth in 5-formyltetrahydrofolate, J. Biol. Chem. 273 (1998) 7873–7879.
[17] A. Tse, K. Brigle, S.M. Taylor, R.G. Moran, Mutations in the reduced folate carrier gene which confer dominant resistance to 5,10-dideazatetrahydrofolate, J. Biol. Chem. 273 (1998) 25953–25960.
[18] K.E. Brigle, M.J. Spinella, E.E. Sierra, I.D. Goldman, Characterization of a mutation in the reduced folate carrier in a transport defective L1210 murine leukemia cell line, J. Biol. Chem. 270 (1995) 22974–22979.
[19] S.C. Wong, L. Zhang, S.A. Proefke, L.H. Matherly, Effects of the loss of capacity for *N*-glycosylation on the transport activity and cellular localization of the human reduced folate carrier, Biochim. Biophys. Acta 1375 (1998) 6–12.
[20] P.L. Ferguson, W.F. Flintoff, Topological and functional analysis of the human reduced folate carrier by hemagglutinin epitope insertion, J. Biol. Chem. 274 (1999) 16269–16278.
[21] D.W. Fry, J.C. Yalowich, I.D. Goldman, Rapid formation of poly-gamma-glutamyl derivatives of methotrexate and their association with dihydrofolate reductase as assessed by high pressure liquid chromatography in the Ehrlich ascites tumor cell in vitro, J. Biol. Chem. 257 (1982) 1890–1896.
[22] S.C. Wong, R. McQuade, S.A. Proefke, A. Bhushan, L.H. Matherly, Human K562 transfectants expressing high levels of reduced folate carrier but exhibiting low transport activity, Biochem. Pharmacol. 53 (1997) 199–206.
[23] R.M. Horton, Z.L. Cai, S.N. Ho, L.R. Pease, Gene splicing by overlap extension: tailor-made genes using the polymerase chain reaction, BioTechniques 8 (1990) 528–535.
[24] L.H. Matherly, C.A. Czajkowski, S.M. Angeles, Identification of a highly glycosylated methotrexate membrane carrier in K562 human erythroleukemia cells up-regulated for tetrahydrofolate cofactor and methotrexate transport, Cancer Res. 51 (1991) 3420–3426.
[25] U.K. Laemmli, Cleavage of structural proteins during the assembly of the head of bacteriophage T4, Nature 227 (1970) 680–685.
[26] P. Matsudaira, Sequence from picomole quantities of proteins electroblotted onto polyvinylidene difluoride membranes, J. Biol. Chem. 262 (1987) 10035–10038.
[27] O.H. Lowry, N.J. Rosebrough, A.L. Farr, R.J. Randall, Protein measurement with the Folin phenol reagent, J. Biol. Chem. 193 (1951) 265–275.
[28] K. Hofmann, W. Stoffel, TMbase—a database of membrane spanning proteins segments, Biol. Chem. Hoppe-Seyler 347 (1993) 166–171.
[29] L.H. Matherly, S.M. Angeles, C.A. Czajkowski, Characterization of transport-mediated methotrexate resistance in human tumor cells with antibodies to the membrane carrier for methotrexate and tetrahydrofolate, J. Biol. Chem. 267 (1992) 23253–23260.
[30] H. Sadlish, R.C. Murray, F.M.R. Williams, W.F. Flintoff, Mutations in the reduced-folate carrier affect protein localization and stability, Biochem. J. 346 (2000) 509–518.
[31] M. Popov, L.Y. Tam, J. Li, R.A. Reithmeier, Mapping the ends of transmembrane segments in a polytopic membrane protein. Scanning *N*-glycosylation mutagenesis of extracytosolic loops in the anion exchanger, Band 3, J. Biol. Chem. 272 (1997) 18325–18332.
[32] I. Nilsson, G. von Heijine, Determination of the distance between the oligosaccharyltransferase active site and the endoplasmic reticulum membrane, J. Biol. Chem. 268 (1993) 5798–5801.
[33] L. Olivares, C. Aragon, C. Gimenez, F. Zafra, Analysis of the transmembrane topology of the glycine transporter GLYT1, J. Biol. Chem. 272 (1997) 1211–1217.

[34] C.J. Pan, B. Lin, J.Y. Chou, Transmembrane topology of human glucose 6-phosphate transporter, J. Biol. Chem. 274 (1999) 13865–13869.
[35] C. Kast, P. Gros, Topology mapping of the amino-terminal half of multidrug resistance-associated protein by epitope insertion and immunofluorescence, J. Biol. Chem. 272 (1997) 26479–26487.
[36] V.A. Canfield, L. Norbeck, R. Levenson, Localization of cytoplasmic and extracellular domains of Na,K-ATPase by epitope tag insertion, Biochemistry 35 (1996) 14165–14172.
[37] A. Warshel, S.T. Russell, A.K. Churg, Macroscopic models for studies of electrostatic interactions in proteins: limitations and applicability, Proc. Natl. Acad. Sci. U. S. A. 81 (1984) 4785–4789.
[38] X. Barril, C. Aleman, M. Orozco, F.J. Luque, Salt bridge interactions: stability of the ionic and neutral complexes in the gas phase, in solution, and in proteins, Proteins 32 (1998) 67–79.
[39] C.N. Chin, G. von Heijine, Charge pair interactions in a model transmembrane helix in the ER membrane, J. Mol. Biol. 303 (2000) 1–5.
[40] R.L. Dunten, M. Sahin-Toth, H.R. Kaback, Role of the charge pair aspartic acid-237–lysine-358 in the lactose permease of *Escherichia coli*, Biochemistry 32 (1993) 3139–3145.
[41] S.S. Gupta, N.D. DeWitt, K.E. Allen, C.W. Slayman, Evidence for a salt bridge between transmembrane segments 5 and 6 of the yeast plasma-membrane H+-ATPase, J. Biol. Chem. 273 (1998) 34328–34334.
[42] A. Merickel, H.R. Kaback, R.H. Edwards, Charged residues in transmembrane domains II and XI of a vesicular monoamine transporter form a charge pair that promotes high affinity substrate recognition, J. Biol. Chem. 272 (1997) 5403–5408.
[43] T. Nakai, A. Yamasaki, M. Sakaguchi, K. Kosaka, K. Mihara, Y. Amaya, S. Miura, Membrane topology of Alzheimer's disease-related Presnilin I. Evidence for the existence of a molecular species with a seven membrane-spanning and one-membrane embedded structure, J. Biol. Chem. 274 (1999) 23647–23658.
[44] D.J. Slotboom, I. Sobczak, W.N. Konings, J.S. Lolkema, A conserved serine-rich stretch in the glutamate transporter family forms a substrate sensitive reentrant loop, Proc. Natl. Acad. Sci. U. S. A. 96 (1999) 14282–15287.
[45] L. Brocke, A. Bendahan, M. Grunewald, B.I. Kanner, Proximity of two oppositely oriented reentrant loops in the glutamate transporter GLT-1 identified by paired cysteine mutagenesis, J. Biol. Chem. 277 (2002) 3892–3985.
[46] S. Frillingos, M. Sahin-Toth, J. Wu, H.R. Kaback, Cys-scanning mutagenesis: a novel approach to structure–function relationships in polytopic membrane proteins, FASEB J. 12 (1998) 1281–1299.